PROCEEDINGS, 49th Workshop on Geothermal Reservoir Engineering
Stanford University, Stanford, California, February 12-14, 2024
SGP-TR-227

On the thermodynamic and economic performance of binary power plant configurations for the exploitation of two-phase geothermal resources

Tristan Merbecks, Dario Alfani, Paola Bombarda, Paolo Silva

Dipartimento di Energia, Via Lambruschini 4, 20156 Milano, Italy

tristanleonard.merbecks@polimi.it

Keywords: organic Rankine cycle, direct steam flash cycle, geothermal fluids

ABSTRACT

Historically, power generation from two-phase and liquid-dominated geothermal resources has been confined to direct steam cycles and binary cycles, respectively. Binary cycles tend to provide a number of operational advantages over direct steam cycles, particularly with regard to the surface handling and reinjection of co-produced high Global Warming Potential non-condensable gases.

However, the design of geothermal power plants for two-phase resources is a demanding task; different technologies, plant configurations and working fluids must be considered, and the optimum plant design is strongly dependent on the geofluid conditions and composition. Moreover, the impact and cost of handling and reinjecting non-condensable gases must be accounted for.

This study investigates the thermodynamic and economic performance of novel binary ORC power plant configurations specifically for two-phase geothermal resources to establish benchmarks against the more commonly adopted flash power plants. A parametric study on the geofluid inlet conditions and NCG content, as well as considering different NCG handling scenarios is conducted to compare their performance and define the optimum application envelope of the different technologies.

1. INTRODUCTION

Geothermal energy is an attractive and versatile option for grid-scale renewable and dispatchable electricity and heat. Direct steam cycles (DSCs) currently represent the majority of geothermal electricity generation capacity (3.67 GW in the US in 2021, representing 67.3% of installed nameplate capacity (Robins et al., 2021)), however binary organic Rankine cycles (ORCs) have allowed the industry to exploit lower enthalpy and otherwise uneconomic geothermal resources (DiPippo, 2016).

The presence of non-condensable gases (NCG) in the geofluid poses a particular challenge in the operation of direct steam cycle power plants. This is because the re-pressurization to atmospheric pressure, as well as processing to remove harmful substances, like hydrogen sulfide and mercury, to make them save to be vented to the atmosphere, is both energy-intensive and expensive. Moreover, carbon dioxide and methane, common constituents of NCG, are potent greenhouse gases with high global warming potential and should ideally not be released to the atmosphere, however the costs of reinjecting NCG are currently prohibitive.

On the other hand, binary ORCs could improve the exploitation of such NCG-rich geothermal resources, as the difference in geothermal fluid pressure across the binary plant is negligible compared to direct steam cycle power plants. Additionally, binary ORCs also provide several other operational advantages over direct steam cycles, such as smaller, cheaper, and more durable turbines as well as a closed loop cycle configuration, which minimize contact of critical plant equipment with the potentially corrosive geofluid. In this respect, extending the application envelope of ORCs is not only of commercial interest but also has the potential to accelerate geothermal energy utilization, contributing to the decarbonization of the energy sector.

2. OBJECTIVES

This study aims to:

- Investigate the exploitation of two-phase geothermal resources using DSC and binary ORC power plants.
- Assess their thermodynamic and techno-economic performance for a range of inlet temperatures and vapor qualities.
- Evaluate how the performance is impacted by the CO_2 content of the geofluid.

3. PLANT CONFIGURATIONS

Two geothermal power plant technologies are considered in this work: direct steam cycles and binary organic Rankine cycles. Irrespective of the power plant technology, for s sound comparison, the system boundaries are defined as the production wellhead and the reinjection facilities inlet. Unless otherwise specified, all geofluid streams are delivered to the reinjection facilities at a pressure equal to that at the production wellhead (i.e., geofluid inlet pressure).

3.1 Direct Steam Cycle

The hot geofluid is "flashed" (i.e., expanded via an expansion valve) to increase its vapor content and then passed through a separator to split the liquid brine and vapor phases (Figure 1) into streams. The vapor is then expanded in a turbine connected to an electrical generator, producing electricity, before being cooled in the condenser, yielding a water-rich condensate stream and an NCG-rich gas stream. The brine and condensate streams are re-pressurized, by means of pumps, and sent to the reinjection facilities. Meanwhile, the NCG stream is re-pressurized by means of a compressor and, depending on the scenario, either vented to the atmosphere or sent to the reinjection facilities. Venting NCG to the atmosphere is evaluated as the reference case.

3.2 Binary Organic Rankine Cycle

The hot geofluid heats and evaporates a secondary high-pressure low-boiling point fluid (Figure 2), the cycle working fluid – typically a hydrocarbon like n-butane or n-pentane or hydrofluorocarbon (HFC) as R134a or R245fa, although the latter are currently being phased out due to concerns over their Ozone Depleting Potential. The resulting high-pressure vapor is expanded in a turbine which drives an alternator, generating electricity. The expanded vapor is then condensed, re-pressurized and returned to the pre-heater. The cold geofluid is re-pressurized and sent to the reinjection facilities. For the purposes of this study the working fluid is assumed to be n-butane.

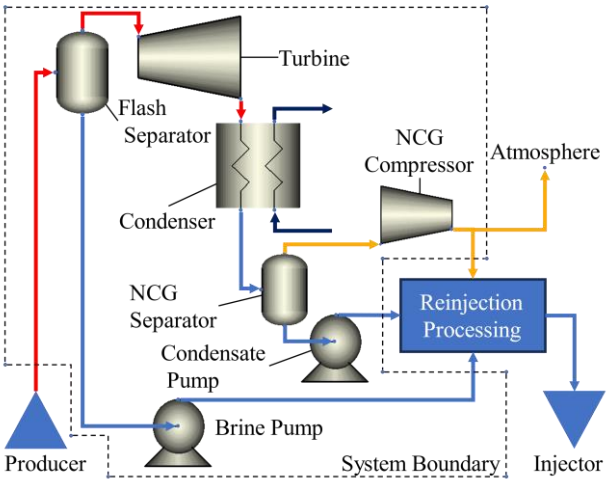

Figure 1 Geothermal DSC geothermal power plant.

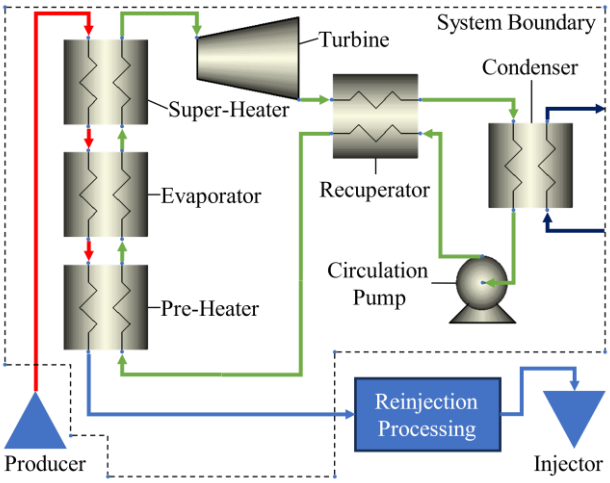

Figure 2 Geothermal binary ORC geothermal power plant

4. MODEL DESCRIPTION

To analyze the performance of these different power plant configurations, an optimization model of the geothermal power plant was created:

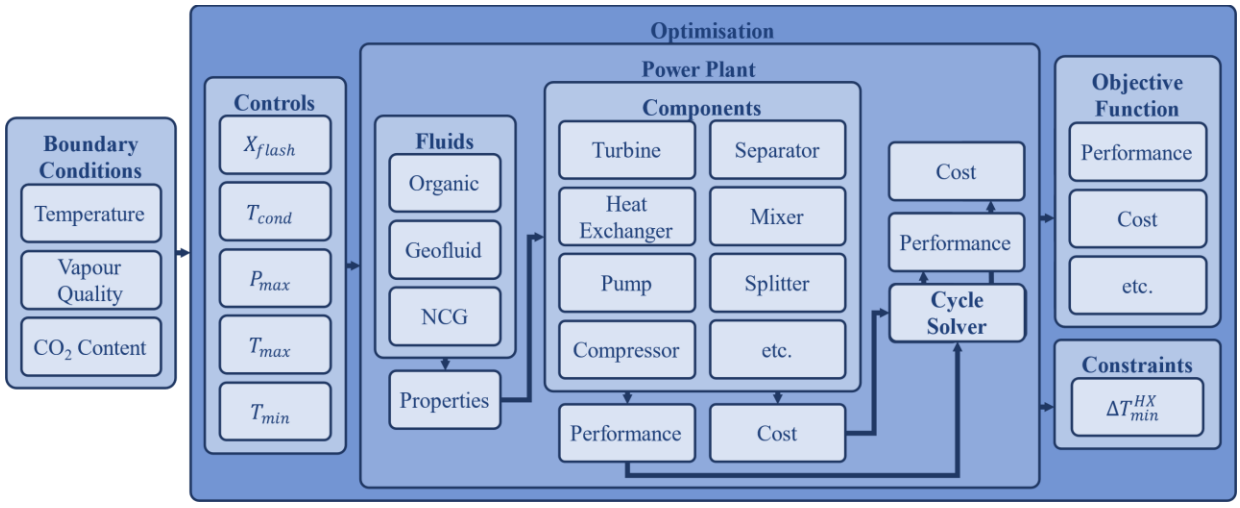

Figure 3 Architecture of the model used to analyze the performance of direct steam cycle and binary ORCs.

4.1 Fluid Descriptions

The thermophysical properties of pure fluids, such as water (i.e., a proxy for geofluids without any NCG content) or n-butane in the binary ORC power plant are modelled using the open-source thermophysical property modelling library *CoolProp* (Bell et al., 2014).

The thermophysical properties of NCG-rich geofluids (assuming that NCG is 100% carbon dioxide) are modelled using a novel, yet to be published, thermophysical property modelling framework, *GeoProp*. In essence, the phase partitioning (i.e. the amount and composition of the equilibrium phases) is calculated via a model by Spycher & Pruess (2009) and the thermophysical properties of the water-rich and carbon dioxide-rich phases are then calculated using *ThermoFun* (Miron et al., 2021) and *CoolProp* respectively.

4.2 Thermodynamic Performance

To model the two power plant configurations, models for the various plant components were defined.

4.2.1 Turbomachinery

The power output (turbine) or consumption (pumps, compressors) of the plant turbomachinery, $\dot{W}$, is calculated through equation (1), where $\dot{m}$ is the mass rate, while h_{in} and h_{out} as well are the specific enthalpy of the fluid at the inlet and outlet of the component, respectively. The outlet enthalpy h_{out} is computed with either equation (2) or (3), depending on the type of equipment. Essentially, an isentropic expansion/compression is simulated down/up to h_{out}^{is}, the isentropic outlet enthalpy, and then corrected using the corresponding definition of the isentropic efficiency, η_{is}.

$$\dot{W} = \dot{m} \cdot (h_{in} - h_{out}) \tag{1}$$

Turbine: $$\eta_{is,turb} = \frac{h_{in} - h_{out}}{h_{in} - h_{out}^{is}} \tag{2}$$ Pump/Compressor: $$\eta_{is,pump/comp} = \frac{h_{out}^{is} - h_{in}}{h_{out} - h_{in}} \tag{3}$$

In the case of steam turbines, the Baumann Rule (Baumann, 1921; DiPippo, 2016) is used to correct $\eta_{is,turb}$ for the formation of liquid droplets within the turbine, (4). Where $\eta_{is,turb}^{dry}$ is the isentropic efficiency of a dry expansion, assumed to be 85 %, while x_{in} and x_{out} are the vapor quality at the turbine inlet and outlet respectively.

$$\eta_{is,turb} = \eta_{is,turb}^{dry} \cdot \frac{x_{in} + x_{out}}{2} \tag{4}$$

The re-pressurization of NCG in the DSC power plant requires large compression ratios (e.g., 200 for a compression from 0.1 bar to 20 bar), which would lead to excessive heating of the NCG. To prevent over-heating, the compression is split into N stages with equal compression ratio, with inter-stage cooling. The number of stages is determined iteratively to avoid outlet temperatures above 473 K (200°C).

4.2.2 Heat Exchangers

The thermal duty of each heat exchanger (i.e. preheater, evaporator, superheater, recuperator and condenser) is calculated by performing a mass and an energy balance (5), while ensuring that the temperature difference between the hot and cold fluid is positive and larger than a pre-defined minimum (i.e. the pinch temperature difference). $\dot{m}^{hot}$ and $\dot{m}^{cold}$ are the mass rates of the hot and cold fluid, h_{in}^{hot} and h_{out}^{hot} as well as h_{in}^{cold} and h_{out}^{cold} are the specific enthalpy of the hot and cold fluids at the inlet and outlet of the heat exchanger.

$$\dot{m}^{hot} \cdot \left(h_{in}^{hot} - h_{out}^{hot}\right) = \dot{m}^{cold} \cdot \left(h_{out}^{cold} - h_{in}^{cold}\right) \tag{5}$$

4.2.3 Other Equipment

All other equipment such as separators and stream mixers perform a mass and energy balance on the inlet and outlet streams.

4.3 Equipment Costs

The plant costs were split into two categories, the primary equipment cost (i.e., the main components of the direct and binary cycle) and the secondary equipment (i.e., minor components like mixers and separators as well as pipping, wiring, control system and construction). The primary equipment costs are evaluated from equipment specific cost correlations, outlined below, while the secondary equipment and construction costs are estimated to represent between 60 – 70% of the total plant cost (Astolfi et al., 2014). For this study, $X_{sec\,\&\,constr}$ takes a value of 2.1.

$$C_{total} = (1 + X_{sec\,\&\,constr}) \cdot C_{primary} \tag{6}$$

The primary equipment cost is calculated as the sum of the primary equipment in the reference year (assumed to be 2019 in this study) and currency (assumed to be USD), (7). As the individual cost correlations have been developed at different points in time and in currencies, the calculated cost must be corrected to the reference year and currency. By convention, the currency is converted to the reference currency in the year of publication of the correlation (8) and then corrected for inflation using the ratio of the Producer Price Index (PPI) of the corresponding equipment in the reference and publication year (9). The USD-EUR exchange rate and PPI values are shown in Figure 4 and Figure 5.

$$C_{primary} = \sum_{i=1}^{N} corr_{PPI} \cdot corr_{currency} \cdot C_i \tag{7}$$

$$corr_{currency} = \frac{USD\,(year_{pub})}{EUR(year_{pub})} \quad (8)$$

$$corr_{PPI} = \frac{PPI\,(year_{ref})}{PPI\,(year_{pub})} \quad (9)$$

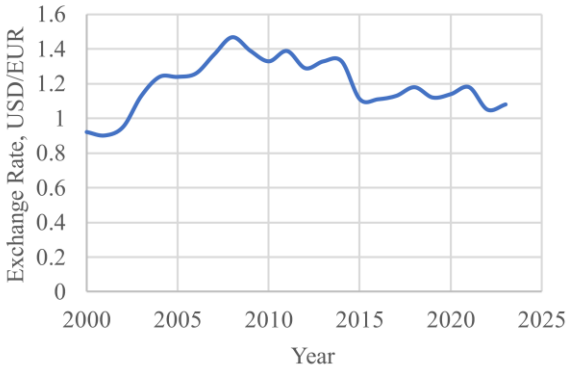

Figure 4 the USD-EUR exchanger rate between 2002 and 2023 (Macrotrends LLC, 2024)

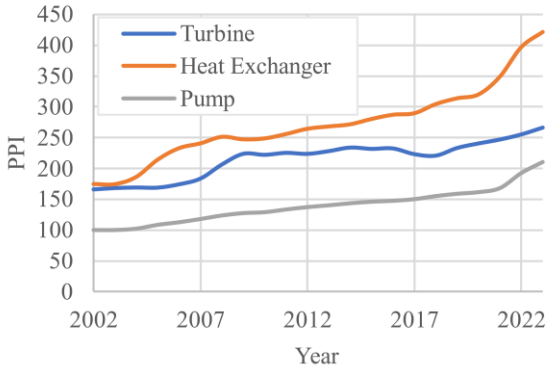

Figure 5 the PPI for turbines (WPU1197), heat exchangers (WPU1075) and pumps/compressors (PCU33391-33391) between 2002 and 2023 (U.S. Bureau of Labor Statistics, 2024)

2.3.1 ORC Turbine

To capture the effect of different working fluids on the cost of the ORC turbine a correlation by Astolfi et al. (2014) was used (10), which correlates the cost, C_{turb}, to the number of stages, n_{stages}, (11) and the size parameter, SP, (12) of the turbine – representative of the turbine length and width, respectively. The cost of the associated generator, C_{gen}, was calculated using equation (7), (Astolfi et al., 2014).

Where Δh_{is}^{tot} is the isentropic enthalpy change across the turbine, Δh_{stage}^{max} is the maximum allowable enthalpy change per stage, $V_{r,is}^{tot}$ is the ratio of inlet and isentropic outlet volume rate, $V_{r,stage}^{max}$ is the maximum allowable isentropic volume rate ratio for a given stage, $\dot{V}_{is}$ is the isentropic volume rate at the turbine outlet, and W_{el} is the electrical power generated by the turbine.

$$C_{turb} = 1.23 \cdot 10^6 \cdot \left(\frac{n_{stages}}{2}\right)^{0.5} \left(\frac{SP}{0.18}\right)^{1.1} €2013 \quad (10)$$

$$n_{stages} = \left\lceil \max\left(\frac{\Delta h_{is}^{tot}}{\Delta h_{stage}^{max}}, \frac{V_{r,is}^{tot}}{V_{r,stage}^{max}}\right)\right\rceil \quad (11)$$

$$SP = \frac{\sqrt{\dot{V}_{is}}}{\sqrt[4]{\frac{\Delta h_{is}^{tot}}{n_{stages}}}} \quad (12)$$

$$C_{gen} = 0.2 \cdot 10^6 \cdot \left(\frac{W_{el}}{5 \cdot 10^6}\right)^{0.67} €2013 \quad (13)$$

2.3.2 Steam Turbine:

A cost model for a wet expansion steam turbine (including generator), $C_{turb+gen}$, was developed (14) from simulated cost data generated with *THERMOFLEX* v31 (Thermoflow Inc., 2021) for a wet expansion steam turbine and associated generator (Figure 6) by changing the inlet temperature and mass flow rate of saturated steam, the condensation pressure was fixed at 10000 Pa.

$$C_{turb+gen} = 1000 * \exp\left(a_1 \cdot ln^2\frac{\dot{W}_{el}}{1000} + a_2 \cdot ln\frac{\dot{W}_{el}}{1000} + a_3\right) * \left(\frac{\dot{V}_{is}^{water+NCG}}{\dot{V}_{is}^{water}}\right)^{0.55} €2021$$
$$a_1 = -0.0408229,\ a_2 = 1.303859,\ a_3 = -0.158304 \quad (14)$$

Where the geofluid vapor contains NCG, an additional correction is applied to capture the effect of the increased volume rate when compared to pure water. The correction follows the definition of the Size Parameter (12), assuming that the isentropic enthalpy change, and number of stages remain constant. In practice, the ratio of the volumetric rate of water and NCG to the volumetric rate of pure water, is approximated as $\frac{1}{1-z_{CO_2}}$, based on the assumption that the two fluids approach ideal gas behaviour at the turbine outlet.

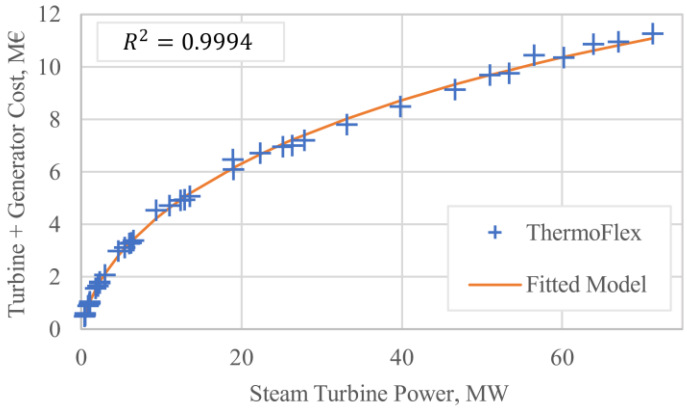

Figure 6 Matched Steam Turbine cost model against cost data generated in *THERMOFLEX* as a function of total turbine power.

2.3.3 Pumps, Fans and Compressors:

The cost of circulation and re-pressurization pumps, C_{pump}, fans, C_{fan}, and NCG compressors, $C_{NCG\ comp}$, are estimated based on the component power, $\dot{W}$, using equations (15), (16) and (17) respectively.

$$C_{pump} = 1185 \cdot \left(1.34 \cdot \frac{\dot{W}}{1000}\right)^{0.767} \text{€2002} \quad \text{(Miles, 2016)} \quad (15)$$

$$C_{fan} = 1.31 \cdot 10^4 \cdot \left(\frac{\dot{W}}{50000}\right)^{0.76} \text{€2005} \quad \text{(Smith, 2005)} \quad (16)$$

$$C_{NCG\ comp} = 6950 \cdot \left(1.34 \cdot \frac{\dot{W}}{1000}\right)^{0.82} \text{€2002} \quad \text{(Duc et al., 2007)} \quad (17)$$

2.3.4 Heat Exchangers

The cost of the recuperator, C_{rec}, where used, is approximated based on the UA of the recuperator (18), with a correction factor for the fluid pressure, f_P, (19) to account for the high wall thickness required (Astolfi et al., 2014). The correction is calculated based on the maximum pressure in the heat exchanger.

$$C_{rec} = 2.60 \cdot 10^5 \cdot \left(\frac{UA}{6.5 \cdot 10^5}\right)^{0.9} \cdot 10^{f_P} \text{€2013} \quad (18)$$

(Astolfi et al., 2014)

$$f_P = a_1 + a_2 \cdot \log_{10}\frac{P}{10^5} + a_3 \cdot \log_{10}^2\frac{P}{10^5} \quad (19)$$

To determine the UA required, the heat exchanger was discretized into $N+1$ points, yielding N segments of equal duty Q^i, and the fluid temperature on the hot and cold side were calculated at each point – this allows the log-mean temperature for each of the N intervals to be determined (20), where ΔT_{in}^i and ΔT_{out}^i are the differences in temperature between the hot and cold side at the inlet and outlet of interval i respectively. Note, where $\Delta T_{in}^i = \Delta T_{out}^i$, ΔT_{lm}^i is assumed to be ΔT_{in}^i. Subsequently, the UA is calculated using (21), where Q^i is the heat transferred in interval i.

$$\Delta T_{lm}^i = \frac{\Delta T_{in}^i - \Delta T_{out}^i}{\ln\frac{\Delta T_{in}^i}{\Delta T_{out}^i}} \quad (20)$$

$$UA = \sum_{i=0}^{N} (UA)^i = \sum_{i=0}^{N} \frac{Q^i}{\Delta T_{lm}^i} \quad (21)$$

For the remaining heat exchangers, the cost is estimated based on the heat transfer area, A. The cost of pre-heaters, evaporators and super-heaters, $C_{Pre-H,\ eva,\ SH}$, is evaluated using equation (22) while the cost of air-cooled condensers, C_{cond}, is calculated from equation (23).

$$C_{Pre-H,\ eva,\ SH} = 239 \cdot A + 1.34 \cdot 10^4 \text{€2002} \quad \text{(Peters et al., 2003)} \quad (22)$$

$$C_{cond} = 1.67 \cdot 10^5 \cdot \left(\frac{A}{200}\right)^{0.89} \text{€2013} \quad \text{(Smith, 2005)} \quad (23)$$

Similarly to above, the heat exchanger was discretized into $N+1$ points, yielding N segments of equal duty, and the temperature and vapor quality on the hot and cold side as well as the log-mean temperature difference (20) were calculated for each point. The vapor qualities, x_{in}^{i} and x_{out}^{i} at the inlet and outlet of interval i, were used to detect any phase changes as well as determine the dominant phase on the hot and cold side of the heat exchanger (24), allowing the appropriate heat transfer coefficient, U^{i}, to be selected from Table 1 and Table 2. The heat transfer area is then calculated using equation (25).

$$Fluid\ type = \begin{cases} Boiling & x_{out}^{i} - x_{in}^{i} > 0 \\ Condensing & x_{out}^{i} - x_{in}^{i} < 0 \\ Liquid & x_{in}^{i} = 0 \\ Vapour & x_{in}^{i} = 1 \end{cases} \quad (24)$$

$$A = \sum_{i=0}^{N} A^{i} = \sum_{i=0}^{N} \frac{Q^{i}}{\Delta T_{lm}^{i} U^{i}} \quad (25)$$

Table 1 Estimated overall heat transfer coefficients U, W/m²/K, in the primary heat exchanger (PHE) for different combinations of fluids and states.

	COLD SIDE	Organic		
HOT SIDE		Liquid	Boiling	Vapor
Water	Liquid	1038	1038	1323
	Condensing	1193	1193	1584
	Vapor	936	936	1161

Table 2 Estimated overall heat transfer coefficients U, W/m²/K, in the air-cooled condenser for different combination of fluids and states.

	HOT SIDE	Organic			Water		
COLD SIDE		Liquid	Condensing	Vapor	Liquid	Condensing	Vapor
Air	Vapor	1048	1089	322	1355	1372	333

4.4 Optimization

The plant performance was optimized using the open-source optimization library *pymoo* (Blank & Deb, 2020) using a genetic optimization algorithm. For the thermodynamic optimization, the net power was selected as the objective function to be optimized, subject to the constraints that the minimum approach temperature difference, ΔT_{min}^{i}, in all heat exchangers is not exceeded (Table 3).

Where $\dot{W}_{net}$ is the net power, ΔT_{min}^{cond}, ΔT_{min}^{Pre-H}, ΔT_{min}^{eva}, ΔT_{min}^{SH} and ΔT_{min}^{rec} are the minimum approach temperature differences in the condenser, pre-heater, evaporator, super-heater and recuperator respectively, P_{out}^{cond} is the condenser outlet pressure, X_{flash} is the degree of geofluid "flashing", T_{out}^{cond} is the condenser outlet temperature, P_{out}^{pump} is the circulation pumps outlet pressure, P_{crit} is the critical pressure of the working fluid and ΔT_{SH} is the degree of working fluid superheating.

Table 3 The optimization parameters for the direct steam cycle and binary ORC power plant

	Direct Steam Cycle	Binary ORC
Objective Function	$\dot{W}_{net}$	$\dot{W}_{net}$
Constraints	$\Delta T_{min}^{cond} \geq 5$ K	$\Delta T_{min}^{cond} \geq 5$ K, $\Delta T_{min}^{Pre-H} \geq 5$ K, $\Delta T_{min}^{eva} \geq 10$ K, $\Delta T_{min}^{SH} \geq 10$ K, $\Delta T_{min}^{rec} \geq 10$ K
Variables	$1 \cdot 10^{4}$ Pa $\leq P_{out}^{cond} \leq 5 \cdot 10^{5}$ Pa $0.3 \leq X_{flash} \leq 1$	303 K $\leq T_{out}^{cond} \leq 400$ K $0.3 \leq \frac{P_{out}^{pump}}{P_{crit}} \leq 0.8$ 3 K $\leq \Delta T_{SH} \leq 15$ K

5. RESULTS

The above model was used to simulate the performance of the direct steam cycle and binary ORC power plants for two cases: 1) the geofluid is assumed to be pure water and 2) the geofluid is assumed to be a mixture of water and CO_2.

5.1 Case 1: Pure Water

The performance of the two power plants was evaluated for geofluid inlet temperatures of 448 K (175 °C), 473 K (200 °C) and 523 K (250 °C) and vapor qualities ranging between 0 to 100 % (i.e., saturated liquid to saturated vapor). The mass flow rate of geofluid was fixed at 50 kg/s. For each set of inlet conditions, the performance of the power plants was optimized for maximum net power.

5.1.1 Thermodynamic Analysis

Comparing the net power produced (Figure 7), it can be seen that while the binary ORC outperforms the direct steam cycle at low vapor qualities, at high vapor qualities the direct steam cycle dominates. The break-even vapor quality, yielding equal net power decreases with increasing temperature. For example, at 448 K the break-even vapor quality is around 45%, it reduces to around 35% at 473 K and 30% at 523K.

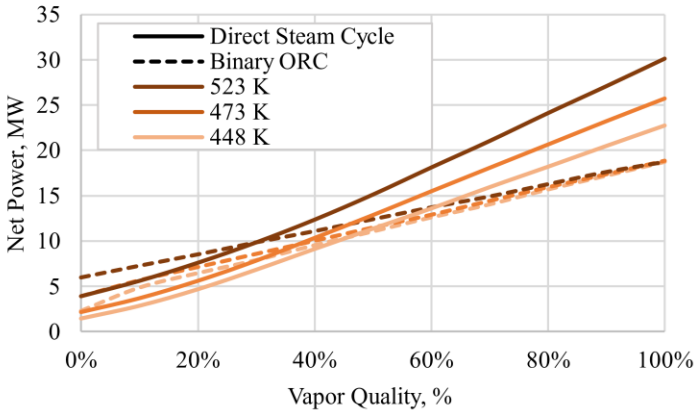

Figure 7 The net power of the direct steam cycle and binary ORC for an inlet mass flow rate of 50 kg/s of pure water as a function of its inlet temperature and steam quality.

The dependence of net power of the binary ORC on the geofluid inlet temperature decrease with increasing vapor quality, as indicated by the convergence on 17.8 MW (for an inlet mass rate of 50 kg/s) for saturated vapor (Figure 7). This can be explained by: a) the specific enthalpy of saturated steam being only weakly dependent on temperature in the range of 200 °C and 250 °C, b) the optimized cycle parameters being virtually identical for all three cases, and c) the pinch-point occurring at the pre-heater hot fluid outlet, as opposed to at the evaporator cold fluid inlet (Figure 8, Figure 9). Consequently, the geofluid outlet temperature and thus the thermal power transferred are fixed in all three cases. As the specific enthalpy change of the working fluid and the PHE thermal power are the same for all three cases, the working fluid mass flow rate is fixed, and in turn the cycle power output.

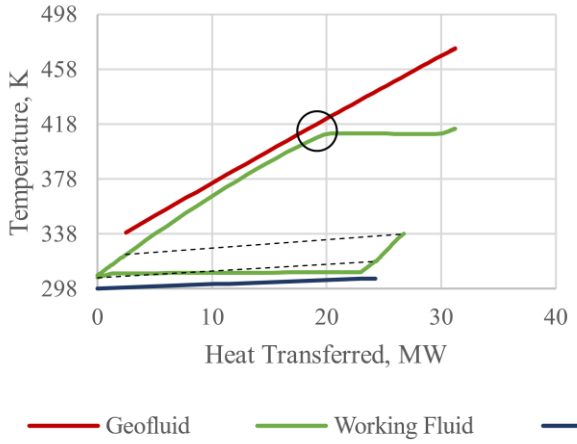

Figure 8 T-Q diagram of binary ORC for 50 kg/s of geofluid at 473 K and vapor quality of 0% (saturated liquid)

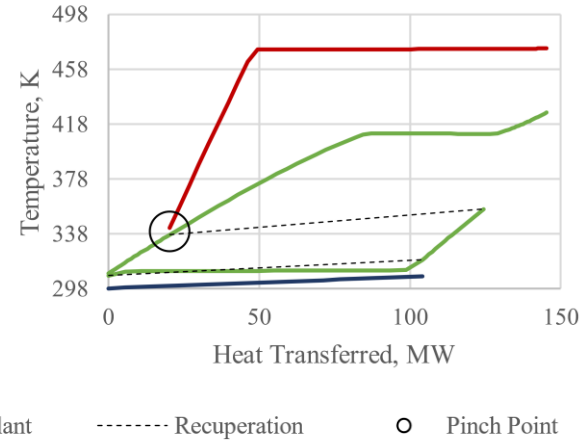

Figure 9 T-Q diagram of binary ORC for 50 kg/s of geofluid at 473 K and vapor quality of 100% (saturated vapor)

5.1.2 Economic Analysis

The specific cost of the primary equipment was calculated for the thermodynamically optimized power plants assuming a geofluid mass rate of 50 kg/s, and it can be noted that the direct steam cycle has a lower specific cost for all geofluid inlet temperatures and vapor qualities considered (Figure 10).

Similarly, the specific cost was also calculated for a range of geofluid mass rates (1 kg/s to 200 kg/s) and all geofluid inlet temperature and vapor quality cases, Figure 11. This allows the specific cost of the power plant to be compared based on the plant capacity instead of on a case-by-case basis, as for each set of geofluid inlet temperature and vapor quality, there exists a combination of mass rates that yield equal net power. Figure 11 shows that there are only a few cases where the binary ORC has a lower specific cost than the DSC.

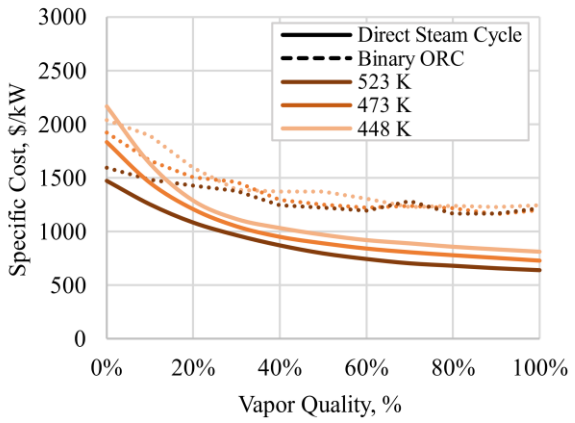

Figure 10 The specific cost of primary plant equipment for direct steam cycle and a binary ORC power plant as a function of geofluid inlet temperature and vapor quality

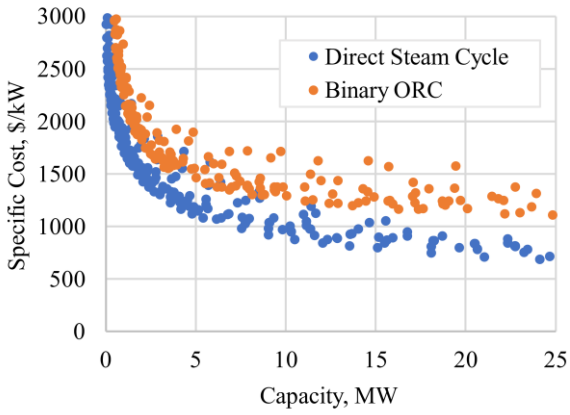

Figure 11 The specific cost of primary plant equipment for direct steam cycle and a binary ORC power plant as a function of plant capacity – for different geofluid inlet temperatures, vapor quality and mass rate

When looking at the breakdown of the primary equipment cost, it can be seen that the turbine and condenser correspond to 80-85% and <95% of the total primary equipment cost for the binary ORC and DSC respectively. The consistently higher condenser cost for the binary ORC can be attributed to the lower heat transfer coefficient compared to pure water (Table 2).

Here it should be noted that the power plants were optimized based on maximum net power, with no regard to the cost of the power plant. Particularly for the binary ORC it could be beneficial (from a cost perspective) to increase the minimum approach temperature difference in the condenser, thus increasing the temperature difference, reducing the heat transfer area required and hence its cost. However, this potentially comes at the cost of turbine power as the condensation pressure (and thus turbine backpressure) would have to be increased. An alternative would be to trial a different cycle working fluid that is better suited to the operating conditions and can thus improve the thermodynamic and techno-economic performance of n-butane.

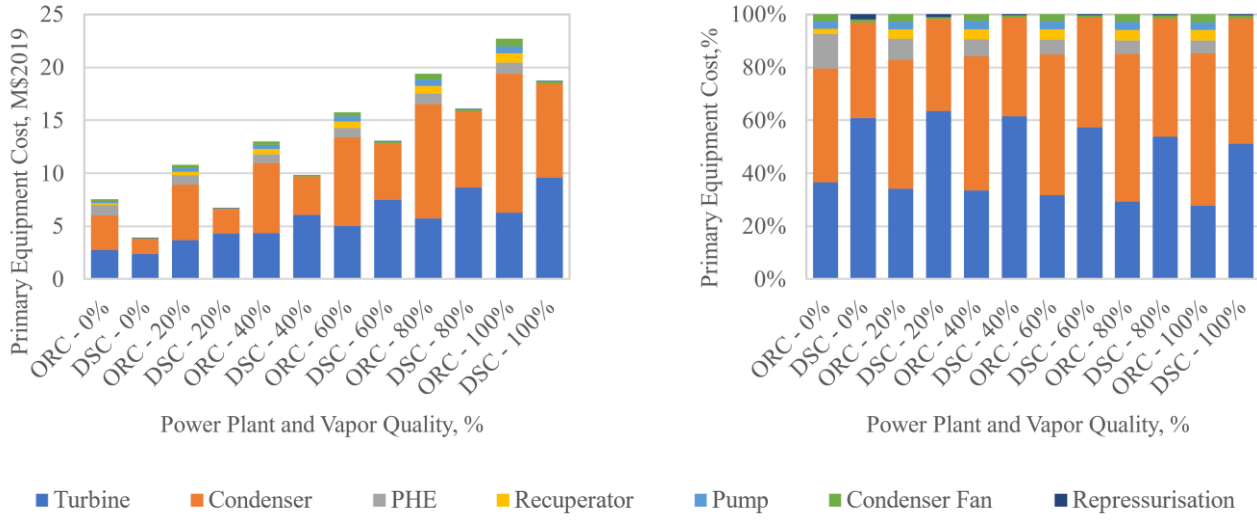

Figure 12 Breakdown of the absolute primary equipment costs for a direct steam cycle and binary ORC power plant as a function of inlet geofluid vapor quality, for a temperature of 473 K (200°C) and a mass rate of 50 kg/s.

Figure 13 Breakdown of the relative primary equipment costs for a direct steam cycle and binary ORC power plant as a function of inlet geofluid vapor quality, for a temperature of 473 K (200°C) and a mass rate of 50 kg/s.

5.2 Case 2: Effect of NCG

To investigate the impact of NCG on the two power plants, their performance was evaluated for geofluids comprised of water and CO_2, CO_2 content between 0 mol% to 12 mol% (0 mass% to 25 mass%). The geofluid inlet temperature was fixed at 473 K (200 °C) and the inlet pressure and vapor quality were determined by ensuring 35% of the water is in the vapor phase, see equation (26) – hereinafter this ratio is referred to as steam quality, where α is the ratio of the amount of species in the vapor phase to the total amount across all phases, y_{H_2O} is the mole fraction of water in the vapor phase and z_{H_2O} is the mole fraction of water in fluid.

To ensure the same thermal power at the power plant inlet for each case, the geofluid mass rate was adjusted to ensure the same thermal power as a mass flow rate of 50 kg/s of pure water entering the plant at a temperature of 473 K and vapor quality of 35%, (27. The superscript *ref* indicates the reference state, corresponding to a pressure of 101325 Pa (atmospheric pressure) and a temperature of 298 K.

$$x_{steam} = \frac{\alpha \cdot y_{H_2O}}{z_{H_2O}} \qquad (26)$$

$$\dot{m}_{geo} = \dot{m}_{water} \frac{h_{water}^{T=473K,\ x_{vap}=0.35} - h_{water}^{ref}}{h_{geo}^{T=473\,K,\ P=P_{in}} - h_{geo}^{ref}} \qquad (27)$$

For the direct steam cycle, two scenarios for the NCG handling were considered: 1) venting the NCG to the atmosphere and 2) reinjecting the NCG into the reservoir. For scenario 1) the vapor is re-pressurized to atmospheric pressure (101325 Pa), while for scenario 2) it is re-pressurized to the geofluid inlet pressure. For the binary ORC, re-pressurization is not required as there are no significant pressure losses in the primary heat exchanger – as such the geofluid outlet pressure is essentially equal to the inlet pressure.

While the reinjection of fluids is not investigated in this study, in reality the geofluid inlet pressure is insufficient to reinject the NCG into the reservoir, as it has a significantly lower density than geofluid in the production wellbore. Nevertheless, Scenario 2 allows for a fairer comparison between the DSCs and binary ORCs, as the subsequent NCG compression (i.e. from P_{in} to $P_{Bottom\,Hole}$) for complete reinjection into the reservoir follows the same compression ratio. The actual power requirement (and thus cost of compressor) may still be different for the two power plants, due to the difference in mass rate of free NCG between the two cases (i.e., CO_2 liberation in flash separator versus cooling of geofluid in primary heat exchangers). This will be investigated in a future study.

5.2.1 Thermodynamic Analysis

Comparing the net power produced by either power plant (Figure 14), it can be seen that the net power of the binary ORC is unaffected by CO_2 content. This is a result of the geofluid inlet and outlet temperature as well as the thermal power carried by the geofluid being constant for all cases, Figure 15. On the other hand, the performance of the direct steam cycle is more strongly dependent on the NCG re-pressurization scenario.

For Scenario 1, where NCG is vented to the atmosphere, the net power can be seen to increase with increasing CO_2 content (about 10% at a CO_2 content of 12 mol% compared to pure water).This increase can be attributed to a) the increased turbine power due to the increasing geofluid inlet pressure with CO_2 content and b) the reduced power requirement for re-pressurizing NCG to atmospheric conditions due to the increasing condensation pressure and thus lower compression ratio.

For Scenario 2, where the NCG is re-pressurized to the geofluid inlet pressure, the net power can be seen to decrease significantly with increasing CO_2 content (about 40% reduction at a CO_2 content of 12 mol% compared to pure water and a 45% reduction when compared to Scenario 1). This can be attributed to the increasing power requirement to re-pressurize the NCG.

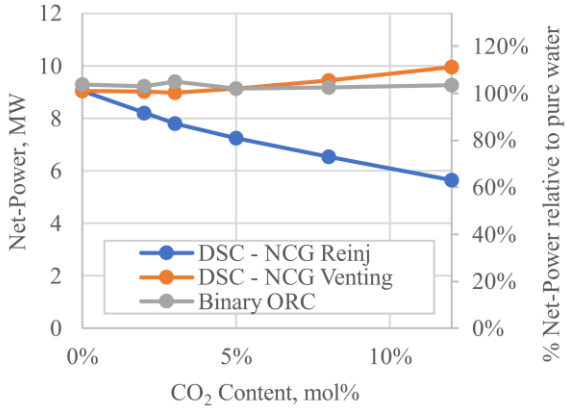

Figure 14 The net power of a DSC and a binary ORC power plant as a function of geofluid CO_2 content for the same inlet temperature and thermal power as 50 kg/s of pure water at 473 K (200 °C) and a vapor quality of 35%

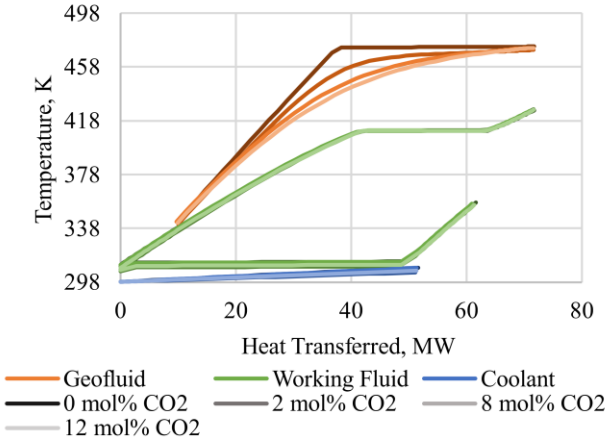

Figure 15 T-Q diagram of binary ORC for geofluids of different CO_2 contents for the same inlet temperature and thermal power as 50 kg/s of pure water at 473 K and vapor quality of 35%.

5.2.2 Economic Analysis

Comparing the primary equipment costs, it can be seen that while the cost of the binary ORC is almost constant, the cost of the direct steam cycle increases significantly for either NCG handling scenario, more than 90% increase for Scenario 1 and 190% increase for Scenario 2. The additional costs can almost entirely be attributed to the cost of the NCG compressor (Figure 17, Figure 18). In terms of primary equipment cost, break-even against the binary ORC is reached for a CO_2 content as low as 1 mol% (2.5 mass%) in Scenario 2 and just over 2 mol% (4.8 mass%) for Scenario 1.

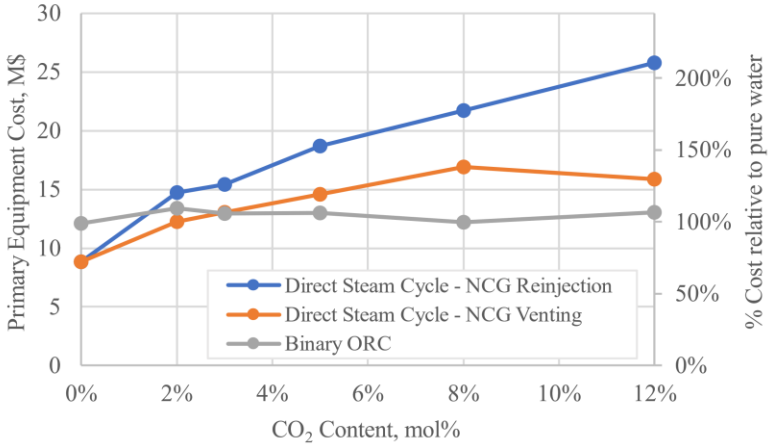

Figure 16 The primary equipment cost of a direct steam cycle power plant and a binary ORC power plant as a function of CO_2 content for a geofluid inlet temperature of 473 K (200 °C), a steam quality of 35% and heat content equivalent of 50 kg/s of pure water at the aforementioned inlet conditions

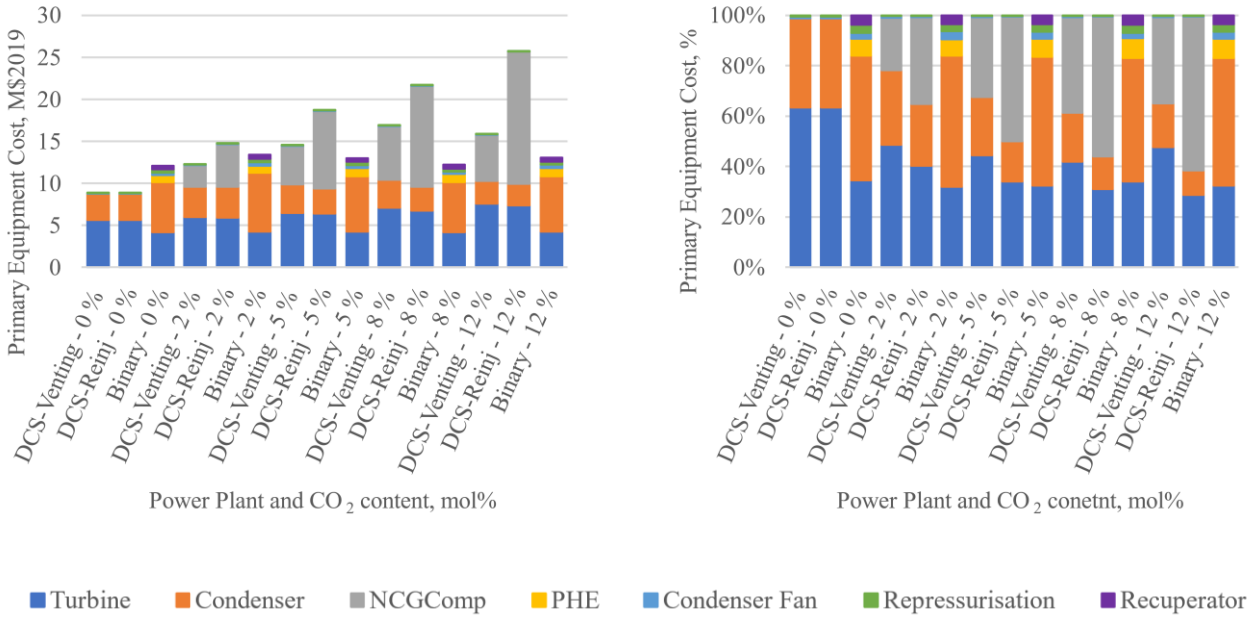

Figure 17 Breakdown of the absolute primary equipment costs for a direct steam cycle and binary ORC power plant as a function of inlet geofluid CO_2 content.

Figure 18 Breakdown of the relative primary equipment costs for a direct steam cycle and binary ORC power plant as a function of inlet geofluid CO_2 content.

The specific primary equipment cost was calculated for a range of geofluid mass rates each power plant, re-pressurization scenario and geofluid CO_2 content (Figure 19). The specific cost of the binary ORC can be seen to be insensitive to geofluid CO_2 content (Figure 19b), while the specific cost of the direct steam cycle increase with CO_2 content and more demanding NCG handling (Figure 19c,d). For CO_2 contents of 2 mol% or higher, the binary ORC can obtain an equivalent or lower specific cost than direct steam cycles with either CO_2 venting or reinject (Figure 19a), for plant capacities between 1 and 20 MW.

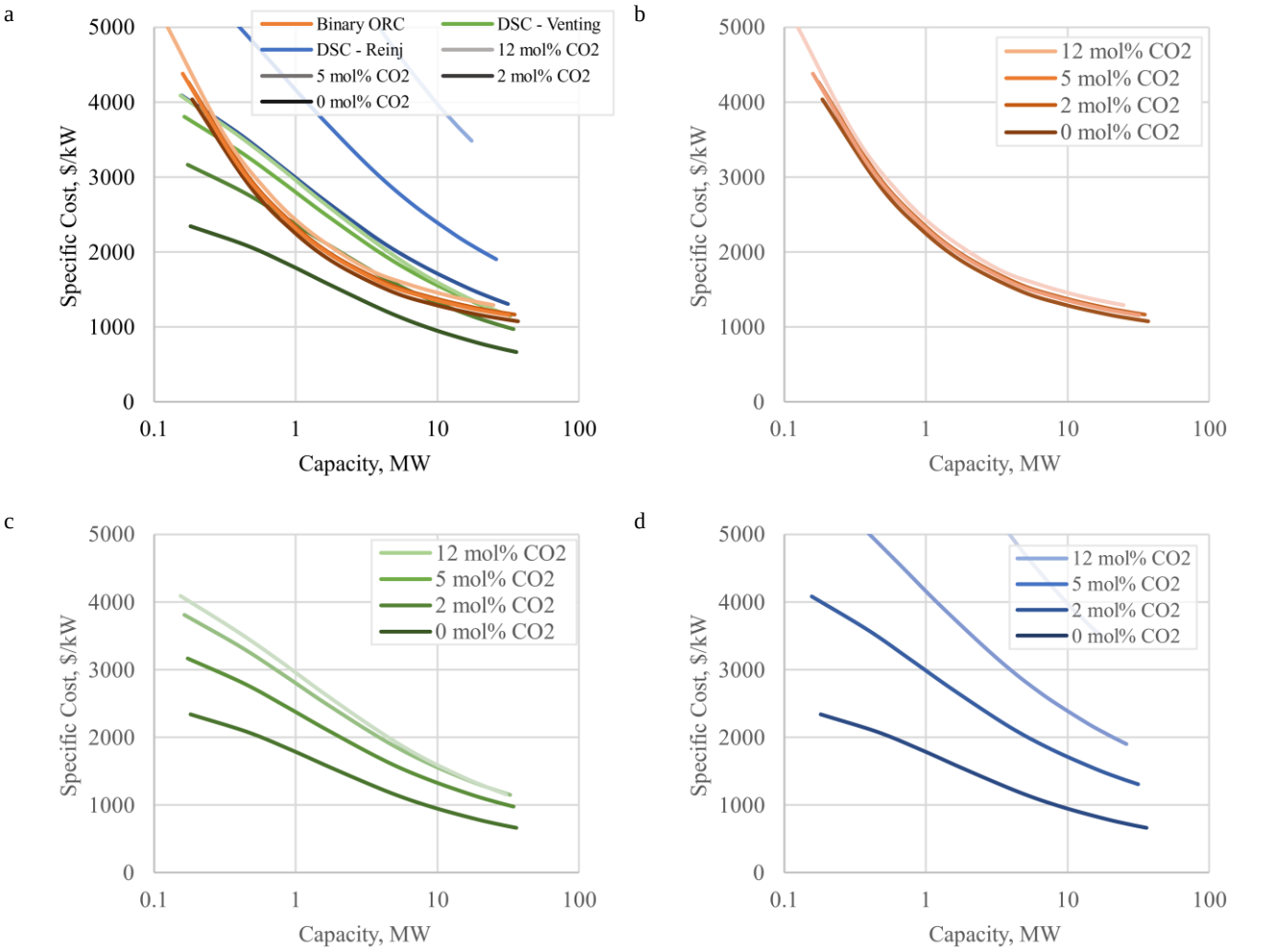

Figure 19 The specific cost of primary plant equipment for direct steam cycle and a binary ORC power plant as a function of plant capacity and geofluid CO_2 contents. Geofluid inlet temperature is 473 K, steam quality is 35% and mass rate is calculated to give equal heat flow relative to pure water at the aforementioned conditions. b, c, d show the plots for the binary ORC, the direct steam cycle with CO_2 venting and CO_2 reinjection, respectively. a is a combination of b, c, and d.

6. CONCLUSIONS

Optimizing net power, simulations of geothermal power plants for a range of two-phase sources showed that binary ORCs operating on n-butane can thermodynamically outperform direct steam cycles, particularly at low to medium vapor quality. However, from a cost perspective the direct steam cycle power plants were seen to provide power at a lower specific cost for all power plant capacities considered. Optimization of the power plant performance based on specific cost or the levelized cost of electricity (LCOE) would be required to identify the optimal techno-economic configuration.

The presence of NCG, in this case CO_2, in the geofluid and its handling has a significant effect on both the thermodynamic and techno-economic performance of the direct steam cycles. While in the case of partial NCG recompression to vent the gases to atmosphere a slight increase in net power is observed, in the case of recompression to the geofluid inlet pressure to have the gas subsequently reinjected into the reservoir, the net power reduces significantly. Moreover, the need for an NCG compressor significantly increases the specific cost of the direct steam cycle power plant in all scenarios studied. For ORCs, the thermodynamic and techno-economic performance are only marginally affected, resulting in the binary cycle outperforming the direct steam cycles on a specific cost basis for geofluid CO_2 contents higher than 2 mol% for a wide range of power plant capacities.

6.1 Future Work

The current results are obtained for a thermodynamically optimized system, which may not correspond to the techno-economic optimum. In this respect, the study should be continued, optimizing the specific investment cost or LCOE. Moreover, the role of other cycle working fluids, such as n-pentane or cyclo-pentane, more complex plant configurations, such as dual-pressure, supercritical, and superheated as well as novel configuration should be investigated. Increasing the range of inlet conditions studied, for example to lower temperature or subcooled conditions will aid in solidifying the application envelope of the two competing technologies.

7. ACKNOWLEDGEMENTS

This project has received funding from the European Union's Horizon 2020 research and innovation program under the Marie Skłodowska-Curie grant agreement No 956965.

This study was carried out within the NEST - Network 4 Energy Sustainable Transition (D.D. 1243 02/08/2022, PE00000021) and received funding under the National Recovery and Resilience Plan (NRRP), Mission 4 Component 2 Investment 1.3, funded from the European Union - NextGenerationEU. This manuscript reflects only the authors' views and opinions, neither the European Union nor the European Commission can be considered responsible for them.

8. REFERENCES

Astolfi, M., Romano, M. C., Bombarda, P., & Macchi, E. (2014). Binary ORC (Organic Rankine Cycles) power plants for the exploitation of medium–low temperature geothermal sources – Part B: Techno-economic optimization. Energy, 66, 435–446. https://doi.org/10.1016/j.energy.2013.11.057

Baumann, K. (1921). Some recent developments in large steam turbine practice. Journal of the Institution of Electrical Engineers, 59(302), 565–623. https://doi.org/10.1049/jiee-1.1921.0040

Bell, I. H., Wronski, J., Quoilin, S., & Lemort, V. (2014). Pure and Pseudo-pure Fluid Thermophysical Property Evaluation and the Open-Source Thermophysical Property Library CoolProp. Industrial & Engineering Chemistry Research, 53(6), 2498–2508. https://doi.org/10.1021/ie4033999

Blank, J., & Deb, K. (2020). pymoo: Multi-Objective Optimization in Python. IEEE Access, 8, 89497–89509.

DiPippo, R. (2016). Geothermal Power Plants (4th ed.). Butterworth-Heinemann. https://doi.org/10.1016/C2014-0-02885-7

Duc, N. H., Chauvy, F., & Herri, J.-M. (2007). CO2 capture by hydrate crystallization – A potential solution for gas emission of steelmaking industry. Energy Conversion and Management, 48(4), 1313–1322. https://doi.org/10.1016/j.enconman.2006.09.024

Macrotrends LLC. (2024). Historical EUR USD exchange rate . https://www.macrotrends.net/2548/euro-dollar-exchange-rate-historical-chart

Miles, G. L. (2016). GETEM User Manual. https://workingincaes.inl.gov/SiteAssets/CAES Files/FORGE/inl_ext-16-38751 GETEM User Manual Final.pdf

Miron, G. D., Kulik, D., Leal, A., & Dmytrieva, S. (2021). ThermoFun: C++/Python code to fetch standard thermodynamic data from ThermoHub database. Goldschmidt2021 Abstracts. https://doi.org/10.7185/gold2021.4489

Peters, M., Timmerhaus, K., & West, R. (2003). Heat-Transfer Equipment _ Design and Costs. Plant Design and Economics for Chemical Engineers (5th ed.).

Robins, J. C., Kolker, A., Flores-Espino, F., Pettitt, W., Schmidt, B., Beckers, K., Pauling, H., & Anderson, B. (2021). 2021 U.S. Geothermal Power Production and District Heating Market Report. https://doi.org/10.2172/1808679

Smith, R. (2005). Chemical process design and integration. In Chemical process design and integration. J. Wiley.

Spycher, N., & Pruess, K. (2009). A Phase-Partitioning Model for CO2–Brine Mixtures at Elevated Temperatures and Pressures: Application to CO2-Enhanced Geothermal Systems. Transport in Porous Media, 82, 173–196. https://doi.org/10.1007/s11242-009-9425-y

Thermoflow Inc. (2021). THERMOFLEX v31.

U.S. Bureau of Labour Statistics. (2024). Producer Price Index. https://www.bls.gov/data/tools.htm